Available online at www.sciencedirect.com

ScienceDirect

journal homepage: www.elsevier.com/locate/he

# Thermodynamic modeling of hydrogen refueling for heavy-duty fuel cell buses and comparison with aggregated real data

*Roberta Caponi* [a,*], *Andrea Monforti Ferrario* [b], *Enrico Bocci* [a], *Gianluca Valenti* [c], *Massimiliano Della Pietra* [b]

[a] *Department of Engineering Science, Guglielmo Marconi University, Via Plinio, 00193, Rome, Italy*
[b] *ENEA, Italian National Agency for New Technologies, Energy and Sustainable Economic Development, C.R. Casaccia TERIN-PSU-ABI, Via Anguillarese, 00123, Rome, Italy*
[c] *Politecnico di Milano, Department of Energy, Via R. Lambruschini 4A, 20156, Milan, Italy*

## HIGHLIGHTS

- A hydrogen refueling 0-D model is developed and applied to heavy-duty vehicles.
- Real case refueling (10 min;half tank) results are within the safety limits.
- Refueling is analyzed for different ambient temperature and vehicle tank pressure.
- The correlation between the refueling time and the refueling speedis non-linear.
- The maximum allowable mass flow rate limits the maximum APRR to 0.08 MPa/s.

## GRAPHICAL ABSTRACT

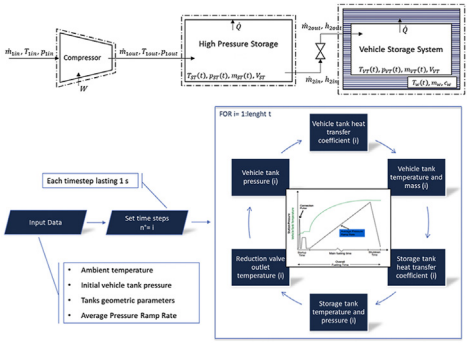


## ARTICLE INFO

*Article history:*
Received 30 November 2020
Received in revised form
17 February 2021
Accepted 28 February 2021
Available online 2 April 2021

*Keywords:*
Hydrogen refueling station
Hydrogen refueling protocol

## ABSTRACT

The foreseen uptake of hydrogen mobility is a fundamental step towards the decarbonization of the transport sector. Under such premises, both refueling infrastructure and vehicles should be deployed together with improved refueling protocols. Several studies focus on refueling the light-duty vehicles with 10 $kg_{H2}$ up to 700 bar, however less known effort is reported for refueling heavy-duty vehicles with 30–40 $kg_{H2}$ at 350 bar. The present study illustrates the application of a lumped model to a fuel cell bus tank-to-tank refueling event, tailored upon the real data acquired in the 3Emotion Project. The evolution of the main refueling quantities, such as pressure, temperature, and mass flow, are predicted dynamically throughout the refueling process, as a function of the operating parameters, within the safety limits imposed by SAE J2601/2 technical standard. The results show to

* *Corresponding author.*
E-mail addresses: r.caponi@lab.unimarconi.it (R. Caponi), andrea.monfortiferrario@enea.it (A. Monforti Ferrario).
https://doi.org/10.1016/j.ijhydene.2021.02.224

Heavy-duty
Thermodynamic modeling
APRR

refuel the vehicle tank from half to full capacity with an Average Pressure Ramp Rate (APRR) equal to 0.03 MPa/s are needed about 10 min. Furthermore, it is found that the effect of varying the initial vehicle tank pressure is more significant than changing the ambient temperature on the refueling performances. In conclusion, the analysis of the effect of different APRR, from 0.03 to 0.1 MPa/s, indicate that is possible to safely reduce the duration of half-to-full refueling by 62% increasing the APRR value from 0.03 to 0.08 MPa/s.



## Introduction

Hydrogen could play a vital role in tackling climate change and become a protagonist in the global energy transition. The reason for this is in its vast potential, as an energy carrier, to connect multiple sectors of the energy matrix, contributing deeply to their decarbonization [1].

Transport is a key sector for which hydrogen is gaining attention, in particular for fueling fuel cell electric vehicles, which are foreseen to become an integral part of the European and national public and private vehicle fleets in the medium-long term [2,3]. Indeed, due to the high energy density of the hydrogen vector, fuel cell vehicles offer long driving ranges, short refueling time, and together with the necessity of just one daily refill, high operational flexibility [4]. For these reasons, fuel cell electric vehicles provide a suitable complementary alternative to battery electric vehicles, which, on the other hand, are more advantageous for urban and light-duty applications due to both required charging infrastructure and vehicle performance issues [2,5,6].

If, as is to be expected [7,8], there will be an evolution of the hydrogen technology on a large scale in the next years, the refueling performances will acquire great importance and thus, the assurance of their understanding and improvement. The SAE J2601 standard regulates the overall fueling process and provides the performance requirements for gaseous hydrogen stations for given operating conditions [9]. These requirements ensure a customer-acceptable and safe refueling since, during the process, the fast fueling may cause gas heating, which may lead to potential hazards.

Two physical phenomena are responsible for this behavior: first, the heat of compression due to the increase of gas pressure inside the tank occurring during the refueling. Second, the reverse Joule-Thomson effect that occurs when hydrogen is throttled since it is characterized by a negative Joule-Thomson coefficient at the temperature and pressure working conditions [10].

Therefore, being able to evaluate the temperature evolution in the tank correctly is of extreme importance. Previous scientific studies focused on determining the temperature distribution within a compressed gas cylinder during refueling, and zero-dimensional models were developed to estimate hydrogen storage systems' overall performance.

Amongst those who adopted this approach, Hosseini et al. [11] dealt with the filling of hydrogen tanks from the perspective of exergy destruction and exergy efficiency, in Striednig et al. [12] ideal gas and real gas simulations are compared, showing that the modeling of the real gas behavior greatly influences the accuracy of the results. Xiao et al. [13,14], applying a lumped parameter model, derived an analytical solution of the temperature and pressure as a function of time. The final formula can fit experimental data and correlate the effects of the process parameters, such as the initial and final masses, initial pressure, mass flow rate, ambient temperature, on the final temperature. The same approach was applied by Zhou et al. [15] to estimate the filling time from different refueling parameters.

In other research, a detailed multi-dimensional heat transfer analysis based on Computational Fluid Dynamics (CFD) was carried out. The multi-dimensional CFD calculations can provide detailed information on the temperature, density, and velocity field within the tank, but the computation requires a high effort level. For example, Dicken and Mérida [16,17] investigated the temperature distribution in a compressed gas cylinder during refueling. Their results, validated by a set of experimental data obtained placing 63 thermocouples in a type III tank, showed a non-uniform temperature distribution during the filling. In contrast, Monde et al. [18–20] demonstrated that the hydrogen in the tank is well stirred and, thus, the temperature can be considered to be uniform. Zhao et al. [10] also performed CFD calculations on temperature rise with good accordance between the numerical simulation and empirical tests. Similar studies have been conducted by de Miguel et al. [21], Guo et al. [22], and Liu et al. [23].

Two main studies analyzed the overall performance of a hydrogen refueling station from a global system point of view. Omdahl [24] developed a dynamic model implemented in MATLAB that includes an electrolyzer, compressors, heat exchangers, storage systems, absorption refrigeration systems, and controllers. In Rothuizen [25], a numerical library developed in Dymola programming environment is used for the modeling of the components. The single-tank and cascade fueling systems are analyzed and then compared from the thermodynamics and energy consumption perspective. NREL (National Renewable Energy Laboratory) studies led to the development of several tools for the simulation of hydrogen

fueling systems. Hydrogen Filling Simulation (H2FillS) is designed to simulate a tank-to-tank refueling of light-duty fuel cell electric vehicles [26]. In contrast, a comprehensive study about the techno-economic feasibility for refueling a fleet of hydrogen fuel cell vehicles was performed by the Hydrogen Station Cost Optimization and Performance Evaluation Model (H2SCOPE), developed by the H2A Analysis Group in collaboration with Argonne National Laboratory [27]. More site-specific techno-economic analyses can be found in literature by Monforti Ferrario et al. [28] and Genovese et al. [29].

In this context, this work presents a zero-dimensional (lumped parameter) thermodynamic model that analyzes the operational performances of the refueling of fuel cell buses. The essence is the assumption that the temperature of the solid is spatially uniform during the transient process [30]. The aim is to provide a description of the behavior of a hydrogen refueling station during a passive tank-to-tank refueling process from a tank storing high-pressure hydrogen at a Nominal Working Pressure (NWP) of 500 bar to a tank at lower pressure, whose NWP is 350 bar. The model results are then compared with aggregate data from real-world refueling stations that are involved in the EU 3Emotion Project. The impact of the variation of ambient temperature, initial vehicle tank pressure, and Average Pressure Ramp Rate (APRR) on the refueling behavior is analyzed via parametric analysis, together with the determination of the most suitable APRR at which the tank system can be filled as fast as possible, within the constraints imposed.

According to the analyzed publications, the majority of the efforts made so far have been focused on the numerical and experimental investigation of the refueling process at small-scale or laboratory scale applications applied to lightweight vehicles application (below 10 kg of hydrogen dispensed, few minutes refueling time, nominal vehicle tank pressure equal to 700 bar). Whilst, a less in-depth investigation has been addressed to refueling heavy-duty vehicles, such as buses or freight vehicles (more than 10 kg refueled per vehicle, longer refueling times between 10 and 20 min, nominal vehicle tank pressure equal to 350 bar). This work is intended to address this gap in the analyzed literature. Although the heavy-duty vehicles 700 bar technology for trucks is gaining interest [31], this paper focuses on the application for 350 bar fuel cell buses with no pre-cooling.

## Thermodynamic model of the refueling of compressed hydrogen tanks

The zero-dimensional thermodynamic model is here presented based on mass and energy balance equations. It is focused on predicting the gas temperature and pressure evolution within the vessels throughout the whole duration of the refueling, with particular regards to the temperature rise within the vehicle vessels, being constrained by safety limits. The whole refueling is simulated according to SAE TIR J2601/2 [32], which applies to gaseous hydrogen powered heavy-duty vehicles. The performance and safety limits are recalled in Table 1.

**Table 1 – SAE J2601/2 safety limits for the refueling of heavy-duty hydrogen vehicles.**

| SAE J2601/2 Fueling Process Limits | |
|---|---|
| Parameter | Limit |
| Ambient temperature range | −40 °C—50 °C |
| Maximum gas temperature | 85 °C |
| Maximum dispenser pressure | 125% NWP |
| Maximum flow rate-normal filling | 0.06 kg/s |
| Maximum flow rate-fast filling | 0.12 kg/s |

### *System overview and assumptions*

The tanks at the station are assumed well-insulated with low thermal conductivity of the liner and, hence, adiabatic [11,12,15,16,33]. The pressure drops were disregarded since their calculation was found not to affect the refueling operation (maximum pressure drop below 1% of NWP), and heat transfer through the piping system is neglected [24]. Fig. 1 depicts a scheme of the analyzed system.

In both the storage tank and vehicle tank, as well as in the tank walls is assumed that the gas temperature, pressure, and density are uniform and stagnant condition prevails. As a consequence, a lumped parameter approach is used to estimate the overall performance of the system. For this hypothesis to be accepted, the Biot number, Bi, defined by the dimensionless quantity $\frac{k_h \delta}{\lambda}$, has to verify the condition $Bi < 0.1$ where, $k_h$ is the convection heat transfer coefficient, $\delta$ is the thickness of the material, and $\lambda$ is the thermal conductivity of the material. The type III tanks studied (metallic linear) showed a $Bi = 0.003$, insofar the lumped system analysis is applicable.

Both tanks' pressures are dynamic, therefore the model is able to handle and describe the hydrogen migration between them. The refueling is governed by the APRR (MPa/s) that defines the desired pressure linear ramp imposed in the vehicle tank. The feed stream is a function of the temperature and pressure change, which is a significant improvement with respect to other analyzed models that consider a fixed inlet flow rate [11,13,15]. In conclusion, an external library named CoolProp [34] is adopted to calculate the thermodynamic properties of the gas at the given state conditions.

### *General equations– mass and energy balances*

For stationary applications, the kinetic and potential energies are usually negligible over the enthalpy, heat, and work rates, hence the first law of thermodynamics, or conservation of energy principle, together with the conservation of mass applied to an open control volume can be written in the form (1) and (2) [11,13,16]:

$$\frac{dU}{dt} = \dot{Q} + \dot{m}_{in} h_{in} - \dot{m}_{out} h_{out} \tag{1}$$

$$\frac{dm}{dt} = \dot{m}_{in} - \dot{m}_{out} \tag{2}$$

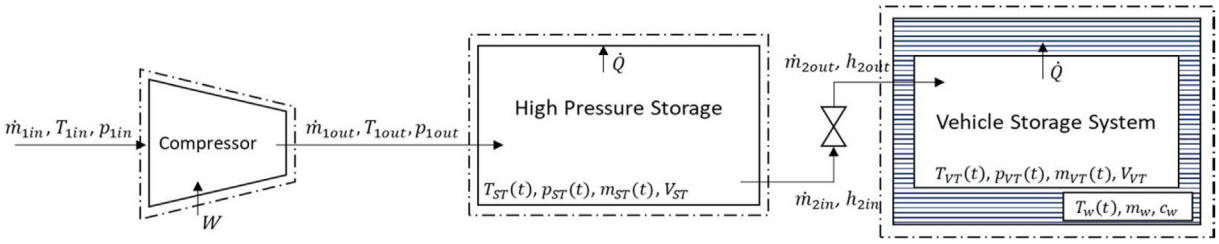


**Fig. 1 – Schematic representation of the modeled hydrogen refueling station including the compressor, the high-pressure storage system, the lamination valve, and the vehicle storage system also showing the tank walls.**

Where $dU/dt$ is the change in internal energy, $\dot{Q}$ is the rate of heat transfer, $\dot{m}_{in}$ and $\dot{m}_{out}$, $h_{in}$ and $h_{out}$ are the hydrogen mass flows and specific enthalpies entering and exiting the control volume respectively, and $dm/dt$ is the rate of accumulation of mass in the control volume.

### *Real gas equation of state*

Due to the high temperature and pressure of refueling a real gas equation is required rather than the ideal gas law, therefore a compressibility factor $Z$ must be introduced. In this study, a virial equation of state [35] is used to define the factor mentioned above:

$$Z = \frac{p\,v}{R_{gas}T} = (1 + Bp) \tag{3}$$

where $R_{gas}$ is the gas constant, equal to 4.124 kJ/kg K, and B is a coefficient that depends on temperature according to the relation, $B = B_1/T + B_2/T^2 + B_3/T^3$.

As stated by the study of Chen et al. Eq. (3) can be truncated at the first term [36] in the temperature range 173 K–393 K. The fitted value becomes $B_1 = 1.9155 \times 10^{-6}$ K/Pa, for which the maximum relative errors introduced are 3.8% respect to the National Institute of Standards and Technology (NIST) data [37]. As a consequence, the real gas equation is as follows:

$$Z = \frac{p\,v}{R_{gas}T} = \left(1 + \frac{B_1 p}{T}\right) \tag{4}$$

Comparable compressibility factor values were found by the authors with the library CoolProp instead of utilizing the analytical expression Eq. (4).

### *Heat transfer*

The gas heating in the tank is moderated by the heat transfer towards the tank walls and the ambient. In this work, the internal heat transfer from gas to the tank wall is considered, whereas the heat exchange from the exterior surface to the surroundings is omitted. This assumption follows the statements of Dicken and Mérida [17], Deymi-Dashtebayaz et al. [38], and Simonovski et al. [39], demonstrating that there is no great variation of the external surface temperature during filling.

For the case of filling high-pressure vessels, there is not a single standard methodology to calculate how the gas exchanges heat with the tank walls and difficulties are faced in the calculation of the convection heat transfer coefficient, $k_h$. Hence, its determination is calculated based on experimental studies and is strongly dependent on geometry, the orientation of the tanks, and the nature of the internal flow. A general approach followed in numerous research [17,18] is to apply a correlation based on dimensionless numbers such that:

$$Nu_{Dint} = \frac{D_{int}\,k_h}{\lambda_{gas}} = aRe_{dint}^{b} + cRa_{Dint}^{d} \tag{5}$$

where $Nu_{Dint}$ is the Nusselt number, defined as the ratio of the thermal energy convected to the fluid to the thermal energy conducted within the fluid calculated over the internal tank diameter, $D_{int}$. The parameters $a$, $b$, $c$ and $d$ are constants whose value is determined upon experimental tests.

In this study, are applied explicit empirical relations of cases with similar operating conditions. Accordingly to the study of Bourgeois [40], for horizontal cylinders for which a zero-dimensional is valid, the correlation for the Nusselt number becomes (Eq. 6):

$$Nu_{dint} = 0.14\,Re_{dint}^{0.67} \tag{6}$$

Therefore, the heat exchange is dominated by the forced convection, which depends on the dimensionless Reynolds number calculated at the inlet of the pressure vessel.

For the case of discharging high-pressure vessels, the reference expression (Eq. (7)) is the correlation developed by Daney [41]. This relation is appropriate for turbulent natural convection in enclosures over the range of the Rayleigh numbers $7 \times 10^8 < Ra_H < 6 \times 10^{11}$.

$$Nu_H = 0.104\,Ra_H^{0.352} \tag{7}$$

The characteristic length for this equation is the cylinder height, $H$, since the high-pressure tanks in the station are placed in a vertical position.

### *Description of components model*

#### *Compressor*

The compressor, for which a quasi-static model based on an isentropic compression transformation is applied, intervenes after completing the refueling process to restore the station

storage nominal pressure. In this work, a two-stage reciprocating compressor with intercooling is modeled.

The equations that allow calculating the electrical compression work and the thermodynamic cooling demand are based on the following assumptions: steady-state conditions ($\dot{m}_{in} - \dot{m}_{out} = 0$), adiabatic compression (Q = 0), and no pressure drops [24].

$$\dot{W} = \dot{W}_{ST1} + \dot{W}_{ST2} = \dot{m}(h_{out} - h_{in})\eta_{el}\eta_{mech} \tag{8}$$

$$\dot{Q}_{IC} = \dot{m}(h_{int2} - h_{int1}) \tag{9}$$

where $h_{in}$ is the specific enthalpy at the inlet conditions of the compressor, $h_{out}$ is the specific enthalpy at the outlet, $h_{int}$ is the specific enthalpy at the outlet of the first stage, $h_{int2}$ is the specific enthalpy at the inlet of the second stage. The assumption of isentropic compression (i.e., $s_{in} = s_{out}$) enables the calculation of the unknown thermodynamic properties. For a reciprocating compressor, the isentropic efficiency is given by Eq. (10) [42]. This equation is valid for compression ratios ($r$) between 1.1 and 5:

$$\eta_{is} = 0.1091(\ln r)^3 - 0.5247(\ln r)^2 + 0,8577 \ln r + 0.3727 \tag{10}$$

*Compressed hydrogen tanks*

The analysis is based on the modeling presented by Xiao et al. [14]. However, the assumption of constant charge or discharge flow is substituted by variable flow, calculated upon the thermodynamic state conditions in each timestep. Indeed, the refueling process is governed by a defined pressure increase given by the APRR (Eq. (11)).

$$\frac{dp_{VT}}{dt} = APRR = constant \tag{11}$$

Considering the process of fueling a tank, therefore analyzing a process with positive inflow, the solution of the mass balance Eq. (2) assuming a constant mass flow at each time, is:

$$m = m_0 + \dot{m}t \tag{12}$$

Combining the energy balance Eq. (1) with Eq. (12) and expressing the rate of heat transfer between the gas and the inner tank wall in terms of convective heat, we obtain:

$$(m_0 + \dot{m}t)\frac{du}{dt} + \dot{m}u = \dot{m}h + k_h A(T_w - T) \tag{13}$$

Defining the characteristic temperature $T^*$ (K) as:

$$T^* = \frac{\gamma T_{in} + \alpha T_w}{1 + \alpha} \tag{14}$$

where $\gamma = c_p/c_v$ is the heat capacity ratio, $T_{in}$ the temperature of the incoming flow, $T_w$ the wall temperature, and $\alpha$ the dimensionless heat transfer coefficient that represents the ratio between the heat transfer intensity and the total heat capacity change:

$$\alpha = \frac{k_h A}{\dot{m}c_v} \tag{15}$$

The equation that describes the evolution of the temperature of the gas in a tank simplifies to:

$$\frac{dT}{dt} = (1 + \alpha)\frac{T^* - T}{t^* + t} \tag{16}$$

Finally, with the initial conditions $T = T_0$ and equal to the ambient temperature at $t = 0$, the solution of the differential equation can be found:

$$T = f_g T_0 + \left(1 - f_g\right)T^* \tag{17}$$

$f_g = (m_0/m)^{(1+\alpha)}$ is the fraction of initial mass over total. The same equations can also be applied for a discharging process, changing the sign of the flow.

While in the storage vessel (much larger volumes implemented), the gas temperature variation is mild for the vehicle vessel (typically of smaller size), the effect of the tank walls and its heating cannot be ignored. The energy balance becomes:

$$\frac{d(m_w c_w T_w)}{dt} = A_{in} k_h (T - T_w) \tag{18}$$

where $m_w$ and $c_w$ refer respectively to the mass of the tank wall and the specific heat of the tank wall. Solving Eq. (18) with the initial condition $T_w = T_{w0}$ at $t = 0$ (at the beginning of each refueling the tanks are in thermal equilibrium with the ambient) can be obtained an analytical expression of the temperature rise in the tank walls.

$$T_w = f_w T_{w0} + (1 - f_w)T \tag{19}$$

Here, $f_w = e^{-\tau_w}$, and $\tau_w$ is a dimensionless time for the tank walls.

*Reduction valve*

The pressure difference between the high-pressure storage tank and the vehicle tank requires the adoption of a reduction valve that regulates the pressure, so that at the outlet the pressure is equal to the identified APRR. Since no work is added and the expansion can be considered adiabatic, the energy balance for a steady-state process describes an isenthalpic process, i.e. $h_{in} = h_{out}$. The effect of hydrogen throttling—calculated via the implementation of CoolProp thermodynamic library known inlet and outlet pressures and constant enthalpy—is an increase in the temperature at the outlet of the valve due to the reverse Joule-Thomson effect.

**Table 2 – Initial filling condition and vehicle tank and storage tank specifications.**

| Input parameter | |
|---|---|
| Ambient temperature, $T_{amb}$ | 15 °C |
| Average Pressure Ramp rate, APRR | 0.03 MPa/s |
| Vehicle tank volume, $V_{VT}$ | 4 × 0.322 $m^3$ |
| Vehicle tank initial pressure, $p_{0,VT}$ | 17.5 MPa |
| Vehicle tank initial temperature, $T_{0,VT}$ | 15 °C |
| Internal diameter of the injector, $d_{int}$ | 0.012 m |
| Storage tank volume, $V_{ST}$ | 11 $m^3$ |
| Storage tank initial pressure, $p_{0,ST}$ | 50 MPa |
| Vehicle tank initial temperature, $T_{0,ST}$ | 15 °C |

### Model implementation

The thermodynamic model developed in this work has been implemented in MATLAB, and an iterative algorithm has been developed to predict the evolution of the refueling parameters within the components throughout the whole refueling duration.

A parametric variation is successfully implemented to the previous algorithm to analyze the effect of different initial temperature, initial pressure, and APRR values on the refueling behavior.

*Algorithms description*

The initial filling conditions and the geometric tank characteristics used in the model are shown in Table 2; the initial conditions are also calibrated in accordance with the real operational parameters of the hydrogen refueling stations (HRS), which are discussed in the following section. The entire refueling is modeled through an iterative procedure in which the initial conditions are determined based on the tanks' initial condition and the thermodynamics at each step are found using the state conditions of the preceding iteration. The setting of the APRR allows the determination of the pressure increase in the vehicle tanks, while the temperature and mass evolution can be found via the real gas equation Eq. (4) and Eq. (17). Due to the mass conservation equation Eq. (2), the inlet and outlet mass flow from each vessel can be derived, which corresponds to a variation of the pressure and temperature respect their initial condition. To resolve the system of equations in each timestep, the MATLAB function *fsolve* was used. The simulation stop criterion corresponds to achieving the full tank capacity, namely reaching 100% state of charge (SOC) of the vehicle.

For the parametric variation, the APRR is not fixed, but the code runs for a range of values (0.03–0.1 MPa/s) and stops when the specified amount of hydrogen to be dispensed is reached or once any of the fueling parameter safety limits have been exceeded. This enables to perform a parametric study on the most suitable ramp rate that enables the refueling in the shortest time possible.

## 3Emotion case study: station characteristics and operational performances

This section presents the operational data [43] for London and Rotterdam HRS sites within the 3Emotion Project, which have been reported via monthly data log files by the site operators and have been collected and successively analyzed by the authors. A summary of the main HRS characteristics of the investigated sites is illustrated in Table 3.

The analyzed data event covers 18 months of operation (January 2018–June 2019) in terms of hydrogen amount refueled (total & by bus), refueling events (time and number), hydrogen dispensed per refueling, refueling duration, daily average resampling, average mass flow rate during refueling. More specific details can be found in the publicly available document [43]. The analysis results can be used both to calibrate the initial conditions and boundary conditions of the model and obtain a high-level aggregate validation of the simulated quantities obtained by the proposed thermodynamic model, showing that the SAE J2601/2 restrictions are not overcome in the transitory of the refueling.

Table 4 summarizes the main numerical results: 57.87 $tons_{H2}$ were dispensed during the analyzed period for over 4128 refueling events. The Rotterdam HRS accounts for just over 15% of the total $H_2$ amount dispensed and refueling events due to the smaller fleet respect to the London site (2 buses vs. 10 buses, respectively). However, the results are balanced in specific terms (hydrogen dispensed by bus and refueling events by bus). With regards to the refueling duration of London buses, the most frequent value (obtained by probability density function analysis with 80% occurrence over the whole sample) is around 9–10 min, which is in line with the project target of 10–12 min; such quantitative analysis could not be performed for the Rotterdam site since the refueling duration is not monitored by the HRS, although a qualitative indication from the site operator has been provided, reporting refueling durations around 12–25 min. The most frequent mass refueled for each refueling (55–60% occurrence) is around 15 $kg_{H2}$/refueling, resulting in equal to around half tank refueling; Fig. 2-a reports the trend of average H2 dispensed by refueling for the two stations over the analyzed period. Fig. 2-b maps the refueling quantity with respect to the refueling duration, showing hotspots for values around 10 min and 15 $kg_{H2}$. Moreover, the hydrogen refueling average flow rate (calculated as dispensed amount divided by total refueling duration) is between 0.027 and 0.03 kg/s, which is compatible with the limitations of the SAE J2601/2 maximum value of 0.06 kg/s.

## Results and discussion

### Vehicle tank refueling process simulation applied to 3Emotion Project

In order to simulate realistic conditions, the model boundary and operating parameters are calibrated according to 3Emotion operation data and relevant literature (Table 2). In particular, an initial tank pressure equal to 17.5 MPa (which

**Table 3 – 3Emotion sites description summary table.**

| Site | Hydrogen source | Capacity [kg/day] | Storage Capacity [kg] | Storage Pressure [bar] | Bus fleet [#] | Gas pressure [bar] |
|---|---|---|---|---|---|---|
| London (UK) | Trucked-in | 400 | 1250 | 350/500 | 10 | 350 |
| Rotterdam (NL) | Pipeline | 200 | 250 | 495/900 | 6 | 350/700 |

**Table 4 – Total (left) and average per bus specific (right) data of dispensed mass and number of refueling events by semester (first semester = H1; second semester = H2) and by site (Rotterdam and London). For Rotterdam only the two buses operated by RET are analyzed.**

| $H_2$ dispensed (kg) | London | Rotterdam (RET) | Total | Specific $H_2$ dispensed (kg/bus) | London | Rotterdam (RET) |
|---|---|---|---|---|---|---|
| H1 2018 | 17,017.39 | 2380.88 | 19,398.27 | H1 2018 | 1701.74 | 1190.44 |
| H2 2018 | 15,831.27 | 3616.93 | 19,448.20 | H2 2018 | 1583.13 | 1808.46 |
| H1 2019 | 16,085.44 | 2947.32 | 19,032.76 | H1 2019 | 1608.54 | 1473.66 |
| Total | 48,934.00 | 8945.13 | 57,879.23 | Total | 4893.40 | 4472.56 |
| Refueling events (#) | London | Rotterdam (RET) | Total | Specific refueling events (#/bus) | London | Rotterdam (RET) |
| H1 2018 | 1188 | 180 | 1368 | H1 2018 | 118.8 | 90 |
| H2 2018 | 1121 | 302 | 1423 | H2 2018 | 112.1 | 151 |
| H1 2019 | 1116 | 221 | 1337 | H1 2019 | 111.6 | 110.5 |
| Total | 3425 | 703 | 4128 | Total | 342.5 | 351.5 |

corresponds to a SOC of 54%) is assumed by considering that the buses are refueled by 16 $kg_{H2}$ (most frequent value according to the analysis of the operational data) up to full tank. This means that the buses always reach full tank capacity during refueling and consume around half tank during service operations, which corresponds to the qualitative information provided by the site bus operators (driving on the upper half of the tank is more likely than driving on the lower half of the

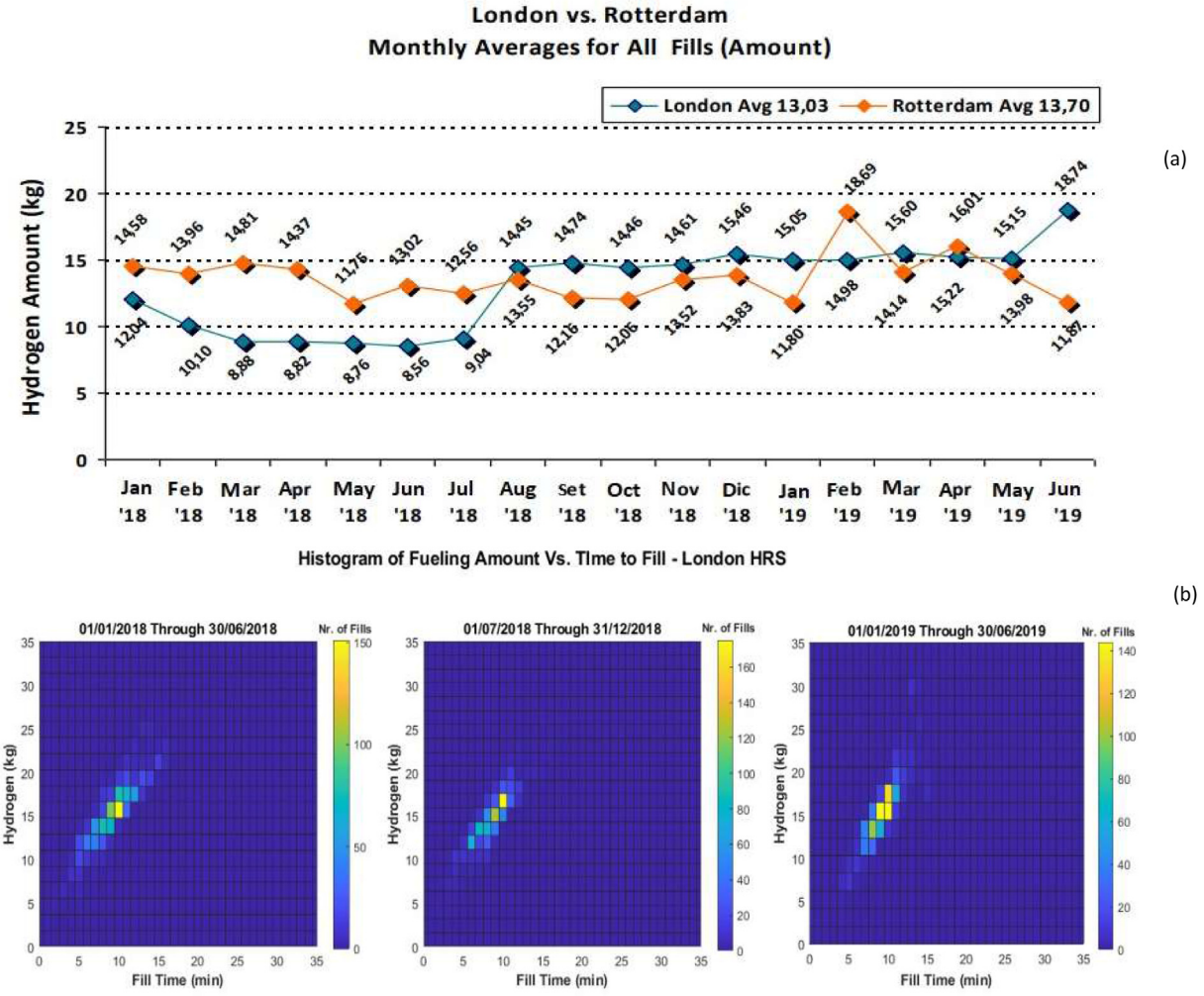


**Fig. 2 – (a) London vs. Rotterdam, monthly average hydrogen dispensed by refueling (kg); (b) refueled amount (kg) vs. duration (min) map.**

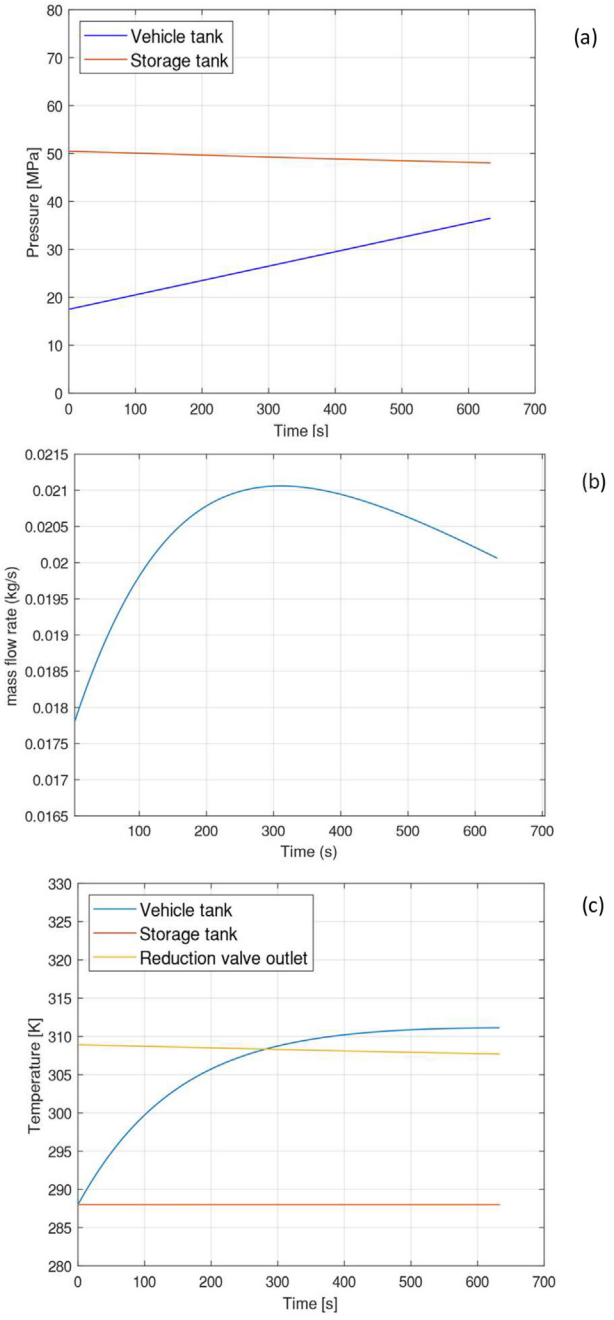


**Fig. 3 – Thermodynamics of hydrogen refueling process over time: pressure (a), mass flow rate (b), and temperature (c) profiles. $T_0 = 15$ °C, $SOC_0 = 54\%$, APRR = 0.03 MPa/s.**

tank, reducing the risk of intra-day unavailability). The storage pressure is equal to the nominal pressure, 50 MPa, assuming that the compressor has fully restored the storage after the preceding refueling event. The ambient temperature for both storage systems—as a first assumption—is considered equal to 15 °C.

The simulation overall results in terms of refueling duration and average mass flow are compared to the available operational data to counter-check the model validity, while

**Table 5 – Comparison between the real operative data of the London station and the results from the model.**

| Average data | 3Emotion - London | Model |
|---|---|---|
| Refueling time | 9.13 min | 10.5 min |
| Mass flow rate | 0.03 kg/s | 0.02 kg/s |
| Mass refueled | 13.03 kg | 14 kg |

the pressure, temperature, and instantaneous mass flow rate dynamic trends are checked to ensure that the SAE J2601/2 limits are not exceeded.

Fig. 3-a shows the gas pressure variation in the two systems. The pressure out of the storage tank decreases due to mass leaving exiting the tank. In contrast, the pressure increases linearly in the vehicle tank at a rate established by the APRR. At the end of the refueling, a target pressure of 36.52 MPa is reached. The refueling time, 633 s (equal to 10.5 min), to reach the target pressure is by all means comparable with the 3Emotion most frequent data.

Fig. 3-b shows the mass flow rate of hydrogen during the charging process. The mass flow is induced by the pressure difference between the two storages and is affected by the state conditions of the gas during the refueling process. Thus it grows in the first part of the refueling, then after a peak of 0.021 kg/s, decreases steadily. In this case, the maximum flow rate imposed by the standard for a normal filling (0.06 kg/s) is never exceeded, and the result is comparable with the average flow rate data collected from the 3Emotion stations' data loggers. A comparison between the real aggregated data form the 3Emotion London station and the model results are illustrated in Table 5.

Fig. 3-c shows the gas temperature evolution in the storage tank, the vehicle tank, and the reduction valve outlet. From the HRS point of view, the gas temperature in the storage tank decreases due to expansion as mass is exiting, although the effect is not very marked due to the larger storage volume of the HRS with respect to the vehicle one. Across the reduction valve, the gas temperature increases caused by the reverse

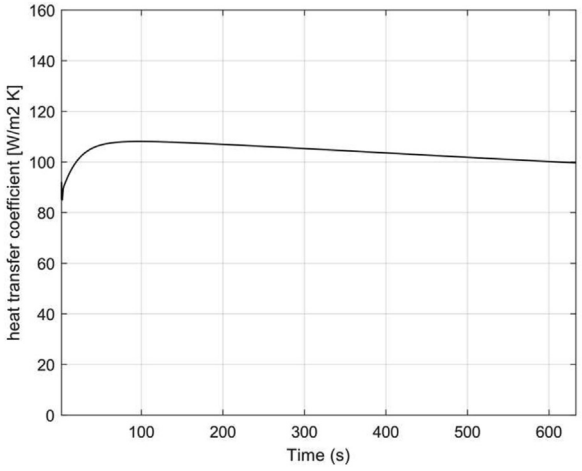


**Fig. 4 – Heat transfer coefficient profile obtained from the model.**

Joule-Thomson effect, moreover, the temperature at the outlet decreases with the evolution of the refueling as a result of decreasing pressure difference between the storages. Lastly, the gas temperature into the vehicle tank increases rapidly at the beginning of the refueling when the system mass flow rate is higher, first leading to a more considerable temperature rise due to compression then flattening to a plateau. The total temperature increment at the end of the refueling is 23.3 °C. The gas temperature in the vehicle tank never reaches the maximum gas temperature limit (358 K) set by the SAE J2601/2.

The overall trends of pressure, mass flow rate, and temperature profiles throughout the tank-to-tank refueling are aligned to what was reported by Rothuizen [25] for 700 bar refueling.

*Heat transfer coefficient evolution*

In Fig. 4, the heat transfer coefficient between the gas and tank wall is plotted throughout a fill process resulting from the application of what discussed in section 'Heat transfer'.

In comparison to what has been predicted in literature [13,17], the convection coefficient increases rapidly within the first seconds, with values up to 100-W/m$^2$ K, and then declines progressively. Indeed, its evolution is strongly related to the rate of mass flow entering the tank: the greater the mass flow rate, the greater is the increase in the coefficient in consequence of higher turbulence at the inlet of the cylinder, that is the cause of the heat exchange. To verify the validity of the heat transfer model, the algorithm has been tested with the data from the study of Bourgeois et al. [40] and the results compared. The curve obtained from the model resembles well the behavior observed by Bourgeois.

*Gas heating: heat of compression and reverse Joule-Thomson effect*

The increase of gas temperature during the process is due to the superposition of the Joule-Thomson effect across the valve and the heat of compression occurring inside the tank. In their study Dicken and Mérida [16] affirm that the latter phenomenon is more significant than the heat generated by the Joule-Thomson effect. In fact, the analysis of the heat exchanged by the gas during the refueling simulated in this work leads to the same conclusions, as showed in Fig. 5.

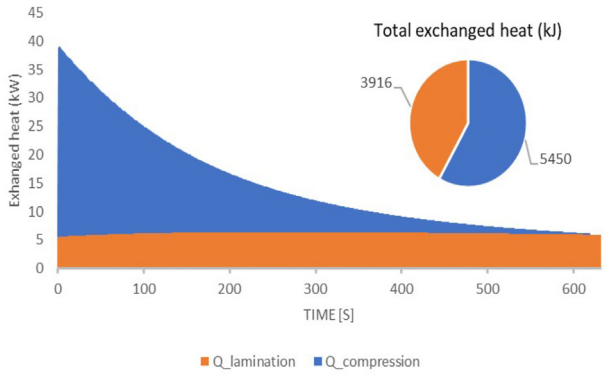


**Fig. 5 – Contributions of the two phenomena, the Joule-Thomson effect, and the heat of compression, that cause the gas heating during the refueling.**

Indeed, 59% of the total exchanged heat is due to the gas compression, while the remaining 41% is due to reverse Joule-Thompson effect. Furthermore, Fig. 5 highlights that the predominance of the heat of compression is exchanged in the initial refueling phase (0–300 s) as more mass enters the vehicle tank corresponding to the greatest increase in the gas temperature.

*Storage tank compression process simulation*

Once the vehicle has been refueled, the HRS storage pressure has decreased due to the exited mass. The restoration of the HRS storage is simulated via the implementation of a displacement compressor, which feeds compressed $H_2$ to the HRS storage. Due to the greater volume capacity the thermodynamic conditions at the station storage do not change significantly. Simulating the refilling of the storage from the initial state, i.e., 48 MPa and 15 °C, back to its nominal conditions (50 MPa), the station takes 1648 s (around 30 min). The refilling time speed strictly depends on the compressor throughput, which is considered constant and equal to 0.0062 kg/s.

The compressor work, calculated as expressed in Eq. (8), increases as the filling advances due to higher pressure ratios in the second stage as the tank pressure reaches the nominal value. Instead, the compressor cooling demand is constant ed equal to 15 kW. The reason is that the operating temperatures of the intercooler are fixed, and the mass flow suctioned by the compressor is also constant.

*Variation of ambient temperature*

The effects of ambient temperature on the temperature distribution within the vehicle tank and the SOC are investigated. The initial pressure is 17.5 MPa, the APRR set to 0.03 MPa/s, while the ambient temperature is varied between 15 and 30 °C. The results are summarized in Table 6.

It can be seen that the temperature profiles (Fig. 6) are almost parallel. Indeed, the temperature difference ΔT between the beginning and the end of the refueling process is approximately the same (between 23 and 24 °C). Furthermore, the higher is the ambient temperature, the greater is the peak.

**Table 6 – Effect of the ambient temperature over final vehicle tank temperature and SOC, and filling time. Initial pressure set at 17.5 MPa.**

| $T_{amb}$ [°C] | Filling time [s] | SOC [%] | Final $T_{VT}$ [K] | $\Delta m_{VT}$ [kg] | ΔT [°C] |
|---|---|---|---|---|---|
| 15 | 633 | 100 | 311.1 | 12.79 | 23.08 |
| 20 | 633 | 100 | 316.4 | 12.65 | 23.38 |
| 25 | 633 | 100 | 321.7 | 12.51 | 23.68 |
| 30 | 633 | 100 | 327.0 | 12.37 | 23.97 |

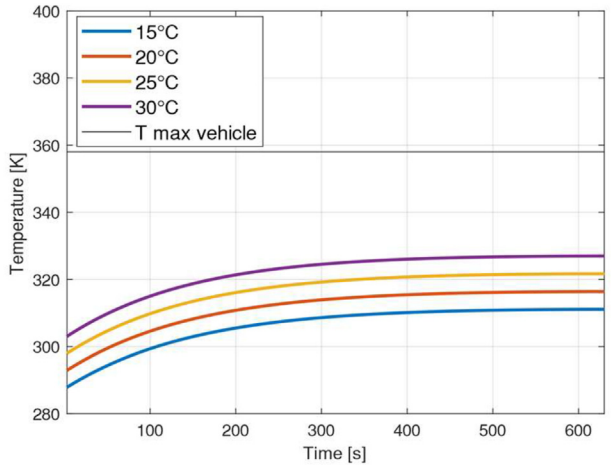


**Fig. 6 – Gas temperature profile at different ambient temperatures between 15 and 30 °C. APRR = 0.03 MPa/s, $p_0$ = 17.5 MPa.**

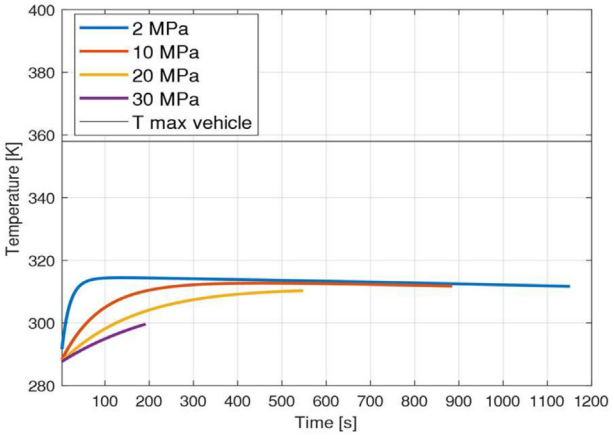


**Fig. 7 – Gas temperature profile at different initial tank pressure between 2 and 30 MPa. APRR = 0.03 MPa/s, $T_0$ = 15 °C.**

This is due to a more significant initial heating of the tank that leads to higher gas temperatures.

Such effects should be carefully considered in operational phase since previous fuel cell bus demo projects highlighted a seasonal performance trend related to ambient temperature. Consequently, HRSs are subject to an increased $H_2$ requirement during winter, especially those located in colder regions [44].

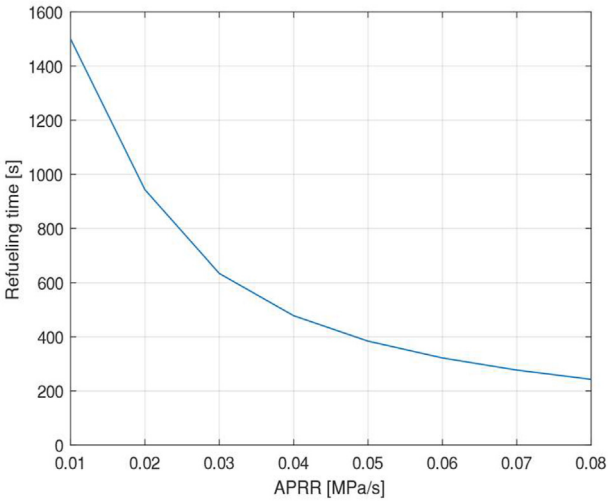


**Fig. 8 – Refueling time versus APRR. $T_0$ = 15 °C, $p_0$ = 17.5 MPa.**

### *Variation of the initial vehicle tank pressure*

In a similar fashion the initial pressure was varied between 2 MPa and 30 MPa while the ambient temperature is fixed at 15 °C. Fig. 7 shows that with decreasing initial pressure the maximum gas temperature in the vehicle tank increases. Indeed, the refueling from 2 MPa to the target pressure results in a more significant increase in temperature (up to 312 K), whereas with an initial pressure equal to 30 MPa, the increase is smaller (up to 300 K).

Therefore, filling with a lower initial pressure yields to a higher overall temperature increment due to refueling time and greater mass filled in the tank (Table 7). Furthermore, a higher initial tank pressure value enhances the achievement of a full tank refueling (SOC equal to 100%), reducing the refueling time and the overall ΔSOC.

A parametric variation over the storage tank initial pressure between 50 MPa and 40 MPa was found to be negligible on the refueling of the vehicle tank (final gas temperature difference below 1%), except when the storage pressure is less than the vehicle NWP, and therefore the SOC equal to 100% cannot be reached.

### *Variation of the APRR*

Finally, the influence of different APRRs is analyzed. The APRR is varied between 0.03 MPa/s to 0.1 MPa/s with an

**Table 7 – Effect of the initial pressure over final vehicle tank temperature, SOC, and filling time. Ambient temperature set at 15 °C.**

| Initial $P_{VT}$ [MPa] | Filling time [s] | Initial SOC [%] | Final SOC [%] | Final $T_{VT}$ [K] | $\Delta m_{VT}$ [kg] | ΔSOC [%] |
|---|---|---|---|---|---|---|
| 2 | 1151 | 5 | 100 | 312.0 | 27.74 | 95 |
| 10 | 885 | 27 | 100 | 311.7 | 19.66 | 73 |
| 20 | 548 | 51 | 100 | 310.3 | 10.63 | 49 |
| 30 | 192 | 72 | 100 | 299.5 | 2.63 | 28 |

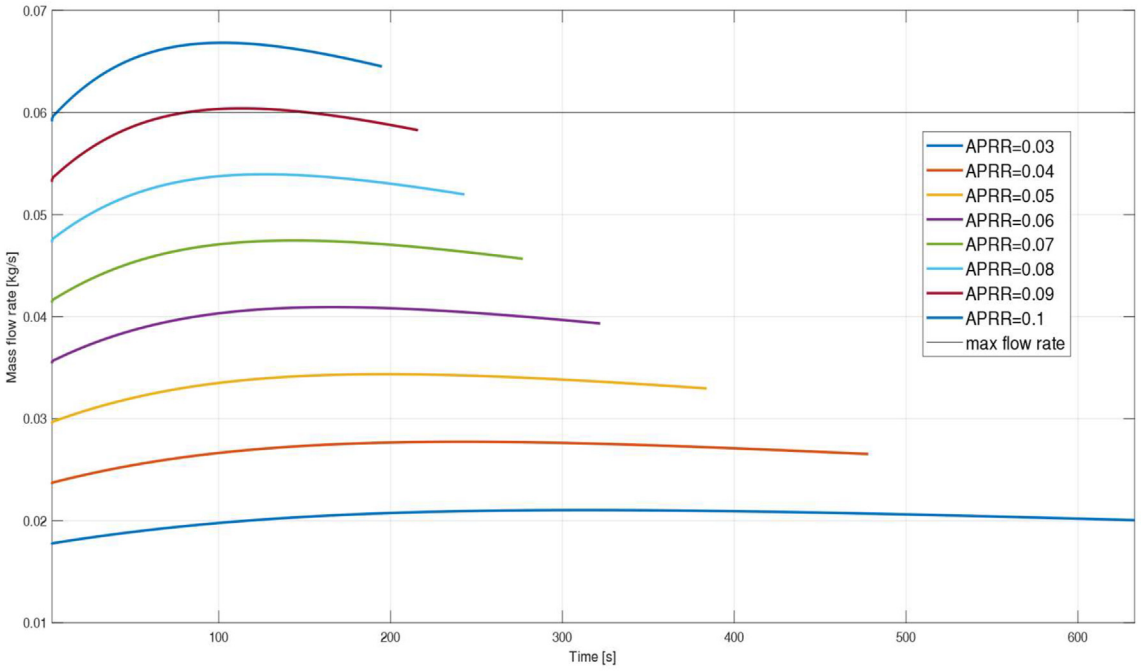


**Fig. 9 – Mass flow rate profile overtime at different APRR between 0.03 and 0.1 MPa/s also showing the maximum flow rate allowed. Simulation up to full tank capacity. $T_0 = 15$ °C, $p_0 = 17.5$ MPa.**

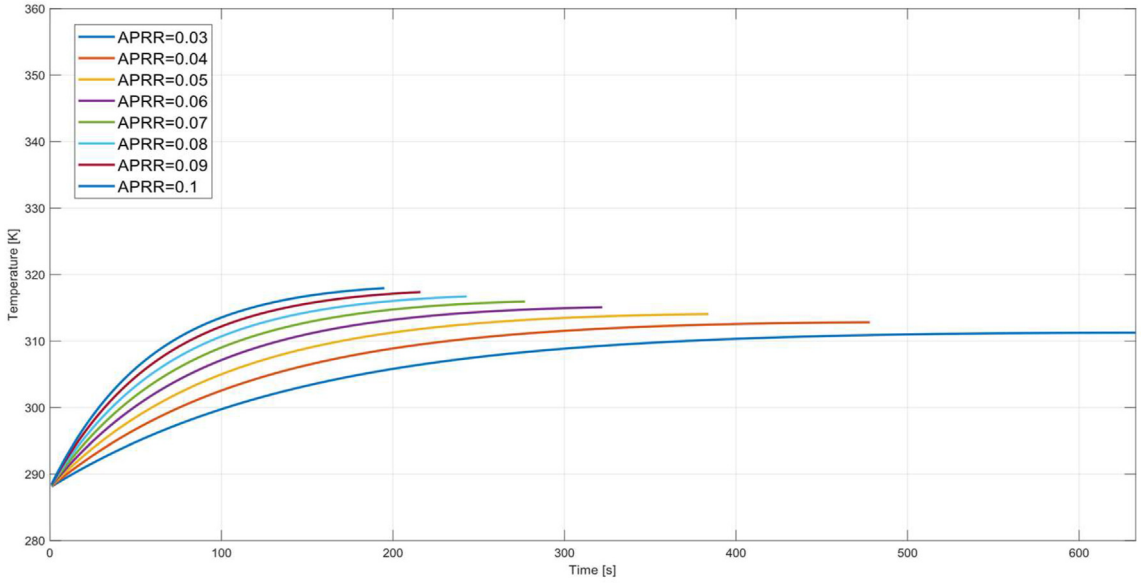


**Fig. 10 – Gas temperature profile overtime at different APRR between 0.03 and 0.1 MPa/s. Simulation up to full tank capacity. $T_0 = 15$ °C, $p_0 = 17.5$ MPa.**

increment of 0.01 MPa/s, while the selected initial conditions are 15 °C and 17.5 MPa. The aim of the parametric analysis is to determine which of those APRRs allow to refuel the vehicle in the shortest time possible while maintaining compliance with the SAE J2601/2 guidelines. Fig. 8 shows the relation between the refueling time and APRR.

As expected, the higher the APRR, the lower the refueling time, although this correlation is not linear. The APRR = 0.08 MPa/s is the highest value that completes the filling without exceeding the safety limits imposed by the SAE J2601/2, as showed in Fig. 9. For this case, the refueling duration is 243 s, which corresponds to a time reduction of about 62%. Finally, temperature profiles under different APRR values are presented in Fig. 10. For each specified APRR, the gas temperature increases and then flattens, but the greater the APRR, the higher the peak that is reached in a shorter time.

## Conclusions

This work provides a thermodynamic analysis of hydrogen refueling stations to fill heavy-duty vehicles. This analysis allow to conclude that:

- The model results are compared with the aggregated data from the 3Emotion Project and with the heat transfer coefficient profile obtained by Bourgeois to demonstrate the correctness of the model.
- Filling the vehicle tank with an APRR = 0.03 MPa/s present a suitable condition in which the pressure, temperature, and density limits given by the SAE J2601/2 are never exceeded. The gas heating in the tank follows a non-linear shape and starting from an ambient temperature of 288 K and an initial pressure of 17.5 MPa, that corresponds to half tank capacity, at the end of the refueling the gas temperature reaches 313.3 K and a target pressure of 36.52 MPa after 633 s.
- The correlation proposed by Bourgeois for modeling the heat transfer in horizontal cylinders filled with high-pressure gas applies well to the case under investigation. This is confirmed by the comparable behavior of the heat transfer coefficient profile calculated in the study and the one obtained from the algorithm tested with the literature data.
- Varying the ambient temperature up to 30 °C increases the final maximum gas temperature in the vehicle tank of 5%. Decreasing the initial vehicle tank pressure down to 2 MPa has a similar effect in terms of final gas temperature in the vehicle tank. Whereas, for greater initial pressures up to 30 MPa, the refueling time, and the ΔSOC considerably decrease – up to 192 s and 28% respectively – due to the lower dispensed mass.
- The filling time and the refueling speed are non-linearly correlated: the lower the first, the higher the second, and hence the APRR that the station should set. For an APRR that is 0.08 MPa/s, the refueling time can be reduced to 243 s, achieving a 62% decrease of the most frequent refueling time obtained from the real operational data, which is equal to 633 s.
- For the analyzed case, the maximum allowable APRR is found to be equal to 0.08 MPa/s. Greater APRR values are not acceptable due to the overcoming of the maximum instantaneous flow rate limit imposed by the SAE J2601/2; in contrast, the gas temperatures in the vehicle tanks do not represent hazardous conditions for any of the analyzed simulations.

The present work can be considered a preliminary study for this type of application. Future work will focus on performing an extensive validation of the model via point-by-point experimental data and extending the modeling of the HRS from a system perspective also considering the production section of the station, increasing the detail in the storage section (cascading multi-pressure systems) or analyzing the interaction with a vehicle fleet (multiple refuelings, refueling scheduling, etc.) rather than a single refueling event.

## Declaration of competing interest

The authors declare that they have no known competing financial interests or personal relationships that could have appeared to influence the work reported in this paper.

## Acknowledgment

This work was supported by CIRPS (Centro Interuniversitario per lo Sviluppo Sostenibile) and the FP7-JTI 3Emotion Project [Grant ID 633174]. The authors would like to thank 3Emotion partners for their collaboration and assistance.

## Nomenclature

| | |
|---|---|
| $A$ | Internal surface area of tank, $m^2$ |
| $B$ | Second virial coefficient, $m^3/mol$ |
| $Bi$ | Biot number |
| $c_p$ | Constant-pressure specific heat, kJ/kg/K |
| $c_v$ | Constant-volume specific heat, kJ/kg/K |
| $c_w$ | Specific heat of tank wall, kJ/kg/K |
| $d$ | Internal diameter of the injector, m |
| $D$ | Internal diameter of the pressure vessel, m |
| $f_g$ | Fraction of initial mass over total mass, $f_g = m_0/m$ |
| $h$ | Specific enthalpy of hydrogen, kJ/kg |
| $k$ | Heat transfer coefficient at inner surface, $kW/m^2/K$ |
| $m$ | Hydrogen mass in tank, kg |
| $m_0$ | Initial mass in tank, kg |
| $\dot{m}$ | Hydrogen mass flow rate, kg/s |
| $m_w$ | Mass of tank wall, kg |
| $Nu$ | Nusselt number |
| $p$ | Pressure of hydrogen, MPa |
| $\dot{Q}$ | Heat transfer rate, kW |
| $r$ | Compression ratio |
| $Ra$ | Rayleigh number |
| $Re$ | Reynolds number |
| $R_{gas}$ | Gas constant, $R_{gas} = 4.124 \times 10^{-3}$ kJ/K/mol |
| $s$ | Specific entropy, KJ/kg/K |
| $t$ | Time variable, s |
| $t^*$ | Characteristic time, $t^* = m_0/\dot{m}$, s |
| $T$ | Temperature of hydrogen, K |
| $T^*$ | Characteristic temperature, $T^*=(\gamma T_{in}+\alpha T_w)/(1+\alpha)$, K |
| $U$ | Internal energy, kJ |
| $u$ | Specific internal energy, kJ/kg |
| $V$ | Tank volume, $m^3$ |
| $v$ | Specific volume, $kg/m^3$ |
| $\dot{W}$ | Work rate, kW |
| $Z$ | Compressibility factor |

*Greek symbols*

| | |
|---|---|
| $\alpha$ | Dimensionless heat transfer coefficient, $\alpha = k_h A/(c_v \dot{m})$ |

| | |
|---|---|
| $\gamma$ | Ratio of specific heats, $\gamma = c_p/c_v$ |
| $\delta$ | Thickness, m |
| | Efficiency |
| $\lambda$ | Thermal conductivity, W/m/K |
| $\tau$ | Dimensionless time, t/t* |

*Acronyms*

| | |
|---|---|
| APRR | Average Pressure Ramp Rate |
| CFD | Computational Fluid Dynamics |
| HRS | Hydrogen refueling station |
| NREL | National Renewable Energy Laboratory |
| NWP | Nominal Working Pressure |
| SAE | Society of Automotive Engineers |
| SOC | State of charge |

*Subscripts*

| | |
|---|---|
| *o* | Initial |
| *amb* | Ambient |
| *el* | Electrical |
| *h* | Convective |
| *H* | Height |
| *H2* | Hydrogen |
| *in* | Inlet |
| *int* | Internal |
| *is* | Isentropic |
| *IC* | Intercooling |
| *mech* | Mechanical |
| *out* | Outlet |
| *RV* | Reduction valve |
| *ST* | Storage tank |
| *ST1* | First stage |
| *ST2* | Second stage |
| *VT* | Vehicle tank |
| *w* | wall |

## REFERENCES


[1] IRENA. Hydrogen: a renewable energy perspective. Abu Dhabi: International Renewable Energy Agency; 2019.

[2] Fuel Cells and Hydrogen Joint Undertaking (FCH JU). Hydrogen roadmap Europe. A sustainable pathway for the European energy transition. https://doi.org/10.2843/249013; 2019.

[3] Piano Nazionale di Sviluppo. Mobilità Idrogeno Italia. 2019;1:1–163.

[4] IEA. The future of hydrogen. 2019. Paris.

[5] California Fuel Cell Partnership. A California road map: the commercialization of hydrogen fuel cell vehicles. 2012.

[6] FCH JU. Fuel cell electric buses-potential for sustainable public transport in Europe. 2015.

[7] IEA. AFC TCP. Survey on the number of fuel cell vehicles. Hydrogen Refueling Stations and Targets; 2019.

[8] Hydrogen Council. Hydrogen scaling up. A sustainable pathway for the global energy transition. 2017.

[9] SAE International. Fueling protocols for light duty gaseous hydrogen surface vehicles (J2601_201612). https://saemobilus.sae.org/content/j2601_201407; 2016.

[10] Zhao L, Liu Y, Yang J, Zhao Y, Zheng J, Bie H, et al. Numerical simulation of temperature rise within hydrogen vehicle cylinder during refueling. Int J Hydrogen Energy 2010;35:8092–100. https://doi.org/10.1016/j.ijhydene.2010.01.027.

[11] Hosseini M, Dincer I, Naterer GF, Rosen MA. Thermodynamic analysis of filling compressed gaseous hydrogen storage tanks. Int J Hydrogen Energy 2012;37:5063–71. https://doi.org/10.1016/j.ijhydene.2011.12.047.

[12] Striednig M, Brandstätter S, Sartory M, Klell M. Thermodynamic real gas analysis of a tank filling process. Int J Hydrogen Energy 2014;39:8495–509. https://doi.org/10.1016/j.ijhydene.2014.03.028.

[13] Xiao J, Bénard P, Chahine R. Charge-discharge cycle thermodynamics for compression hydrogen storage system. Int J Hydrogen Energy 2016;41:5531–9. https://doi.org/10.1016/j.ijhydene.2015.12.136.

[14] Xiao J, Wang X, Zhou X, Bénard P, Chahine R. A dual zone thermodynamic model for refueling hydrogen vehicles. Int J Hydrogen Energy 2019;44:8780–90. https://doi.org/10.1016/j.ijhydene.2018.10.235.

[15] Zhou X, Yang T, Xiao J, Bénard P, Chahine R. Estimation of filling time for compressed hydrogen refueling. Energy procedia, vol. 158. Elsevier Ltd; 2019. p. 1897–903. https://doi.org/10.1016/j.egypro.2019.01.438.

[16] Dicken CJB, Mérida W. Measured effects of filling time and initial mass on the temperature distribution within a hydrogen cylinder during refuelling. J Power Sources 2007;165:324–36. https://doi.org/10.1016/j.jpowsour.2006.11.077.

[17] Dicken CJB, Mérida W. Modeling the transient temperature distribution within a hydrogen cylinder during refueling. Numer Heat Tran Part A: Applications 2008;53:685–708. https://doi.org/10.1080/10407780701634383.

[18] Woodfield PL, Monde M, Mitsutake Y. Measurement of averaged heat transfer coefficients in high-pressure vessel during charging with hydrogen, nitrogen or argon gas. J Therm Sci Technol 2007;2:180–91. https://doi.org/10.1299/jtst.2.180.

[19] Monde M, Woodfield P, Takano T, Kosaka M. Estimation of temperature change in practical hydrogen pressure tanks being filled at high pressures of 35 and 70 MPa. Int J Hydrogen Energy 2012;37:5723–34. https://doi.org/10.1016/j.ijhydene.2011.12.136.

[20] Monde M, Mitsutake Y, Woodfield PLl, Maruyama S. Characteristics of heat transfer and temperature rise of hydrogen during rapid hydrogen filling at high pressure. Heat Tran Asian Res 2007;36:13–27. https://doi.org/10.1002/htj.20140.

[21] de Miguel N, Ortiz Cebolla R, Acosta B, Moretto P, Harskamp F, Bonato C. Compressed hydrogen tanks for on-board application: thermal behaviour during cycling. Int J Hydrogen Energy 2015;40:6449–58. https://doi.org/10.1016/j.ijhydene.2015.03.035.

[22] Guo J, Yang J, Zhao Y, Pan X, Zhang L, Zhao L, et al. Investigations on temperature variation within a type III cylinder during the hydrogen gas cycling test. Int J Hydrogen Energy 2014;39:13926–34. https://doi.org/10.1016/j.ijhydene.2014.03.097.

[23] Liu J, Zheng S, Zhang Z, Zheng J, Zhao Y. Numerical study on the fast filling of on-bus gaseous hydrogen storage cylinder. Int J Hydrogen Energy 2020;45:9241–51. https://doi.org/10.1016/j.ijhydene.2020.01.033.

[24] Omdahl NH. Modeling of a hydrogen refueling station. MSc thesis, MSc thesis; 2014.

[25] Rothuizen E. Hydrogen fuelling stations. A thermodynamic analysis of fuelling hydrogen vehicles for personal transportation. PhD thesis. Danmarks Tekniske Universitet; 2013.

[26] Kuroki T, Nagasawa K, Peters M, Leighton D, Kurtz J, Sakoda N, et al. Thermodynamic modeling of hydrogen fueling process from high pressure storage tanks to vehicle tank n.d. https://www.nrel.gov/hydrogen/h2fills.html..

[27] Elgowainy Amgad, Krishna Reddi, Aly Mohamed. Heavy-duty refueling station analysis model (HDRSAM). https://hdsam.es.anl.gov/index.php?content=hdrsam; 2018.
[28] Monforti Ferrario A, Rajabi Hamedani S, del Zotto L, Santori Simone G, Bocci E. Techno-economic analysis of in-situ production by electrolysis, biomass gasification and delivery systems for Hydrogen Refuelling Stations: rome case study. Energy procedia, vol. 148. Elsevier Ltd; 2018. p. 82–9. https://doi.org/10.1016/j.egypro.2018.08.033.
[29] Fragiacomo P, Genovese M. Technical-economic analysis of a hydrogen production facility for power-to-gas and hydrogen mobility under different renewable sources in Southern Italy. Energy Convers Manag 2020;223. https://doi.org/10.1016/j.enconman.2020.113332.
[30] Bergman TL, Incropera FP, DeWitt DP, Lavine AS. Fundamentals of heat and mass transfer. John Wiley & Sons; 2011.
[31] FCH JU. Fuel cell hydrogen trucks-heavy duty's high performance green solution. https://doi.org/10.2843/168949; 2020.
[32] SAE International. Fueling protocol for gaseous hydrogen powered heavy duty vehicles (J2601/2_201409). https://saemobilus.sae.org/content/j2601/2_201409; 2016.
[33] Rothuizen E, Mérida W, Rokni M, Wistoft-Ibsen M. Optimization of hydrogen vehicle refueling via dynamic simulation. Int J Hydrogen Energy 2013;38:4221–31. https://doi.org/10.1016/j.ijhydene.2013.01.161.
[34] Bell IH, Wronski J, Quoilin S, Lemort V. Pure and pseudo-pure fluid thermophysical property evaluation and the open-source thermophysical property library CoolProp. Ind Eng Chem Res 2014;53:2498–508. https://doi.org/10.1021/ie4033999.
[35] Smith JM, van Ness HC, Abbott MM. Introduction to chemical engineering thermodynamics. McGraw-Hill; 2005.
[36] Chen H, Zheng J, Xu P, Li L, Liu Y, Bie H. Study on real-gas equations of high pressure hydrogen. Int J Hydrogen Energy 2010;35:3100–4. https://doi.org/10.1016/j.ijhydene.2009.08.029.
[37] Lemmon E, Huber M, McLinden. NIST standard reference database 23: reference fluid thermodynamics and transport properties-REFPROP. 9.1. National Institute of Standards and Technology, Standard Reference Library; 2013. https://doi.org/10.1016/0031.
[38] Deymi-Dashtebayaz M, Farzaneh-Gord M, Nooralipoor N, Niazmand H. The complete modelling of the filling process of hydrogen onboard vehicle cylinders. Braz J Chem Eng 2016;33:391–9. https://doi.org/10.1590/0104-6632.20160332s20140209.
[39] Simonovski I, Baraldi D, Melideo D, Acosta-Iborra B. Thermal simulations of a hydrogen storage tank during fast filling. Int J Hydrogen Energy 2015;40:12560–71. https://doi.org/10.1016/j.ijhydene.2015.06.114.
[40] Bourgeois T, Ammouri F, Weber M, Knapik C. Evaluating the temperature inside a tank during a filling with highly-pressurized gas. Int J Hydrogen Energy 2015;40:11748–55. https://doi.org/10.1016/j.ijhydene.2015.01.096.
[41] Daney DE. Turbulent natural convection of liquid deuterium, hydrogen, and nitrogen within enclosed vessels. Int J Heat Mass Tran 1976;19:431–41. https://doi.org/10.6028/NBS.IR.75-807.
[42] Smith R. Chemical process design and integration. 1st ed. John Wiley & Sons; 2005.
[43] Caponi R, Monforti Ferrario A, Bocci E, del Zotto L. DELIVERABLE n. 2.4 Operational HRS performances Report n1. 2020.
[44] FCH JU. Fuel cell buses. HyTRANSIT and HighV. 2019. LO-City, Brussels.